array. Capping with a volatile species (pyridine) permits the removal of the cap by heating at 150°C under vacuum after formation of the array. QDs in such an array are in intimate contact but are not sintered.

Self-organization is a general phenomenon of colloidal dispersions where control over particle size and stabilization has been achieved. Colloidal crystals are not restricted to simple "monatomic" lattice types. Complex binary superlattices with AB_2 structures (A and B are spheres of different radii) have been found in natural opals (*16*). Examples of AB_2, AB_5, and AB_{13} systems have been prepared with synthetic latex spheres (*16*). Composite colloidal solids have been produced with the use of silica and latex spheres (*17*). Similar complex structures of QDs should be possible.

Colloidal self-organization with nanocrystallites is not restricted to semiconductor QDs (*6*). Self-organization requires only a hard-sphere repulsion, a controlled size distribution, the inherent van der Waals attraction between particles, and a means of gently destabilizing the dispersion. Synthetic routes to monodisperse nanocrystallites of insulating, semiconducting, magnetic, and metallic materials are being pursued by many groups. Manipulation of these diverse materials into superlattices as demonstrated for CdSe QDs in this report should be readily accomplished after control over size distributions and stabilization have been established. The rational design of novel and potentially useful superlattice structures with a variety of nanometer-sized building blocks should then be possible.

REFERENCES AND NOTES

1. M. A. Kastner, *Phys. Today* **46** (no. 1), 24 (1993).
2. L. E. Brus, *Appl. Phys. A* **53**, 465 (1991).
3. L. N. Lewis, *Chem. Rev.* **93**, 2693 (1993).
4. R. Freer, *Nanoceramics* (Institute of Materials, London, 1993).
5. D. D. Awschalom and D. P. DiVincenzo, *Phys. Today* **48** (no. 4), 43 (1995); ______, J. F. Smyth, *Science* **258**, 414 (1992).
6. Opals are a natural example of colloidal crystals; their iridescence is a result of Bragg diffraction of light by 3D arrays of monodisperse, micrometer-sized silica particles [J. V. Sanders, *Acta Crystallogr. Sect. A* **24**, 427 (1967)]. P. Pieranski, *Contemp. Phys.* **25**, 25 (1983) and references therein; P. N. Pusey *et al.*, *Phys. Rev. B* **63**, 25 (1989); S. A. Asher, P. L. Flaugh, G. Washinger, *Spectroscopy* **1** (no. 12), 27 (1986). Colloidal crystallization of nanometer-sized colloids has been demonstrated with 70 Å iron oxide particles [M. D. Bentzon, J. van Wonterghem, S. Morup, A. Tholen, C. J. W. Koch, *Philos. Mag. B* **60**, 169 (1989); M. D. Bentzon and A. Tholen, *Ultramicroscopy* **38**, 105 (1990)].
7. T. Takagahara, *Optoelect. Dev. Tech.* **8**, 545 (1993); *Surf. Sci.* **267**, 310 (1992).
8. D. Heitmann and J. P. Kotthaus, *Phys. Today* **46** (no. 1), 56 (1993).
9. C. B. Murray, D. J. Norris, M. G. Bawendi, *J. Am. Chem. Soc.* **115**, 8706 (1993).
10. L. Becerra, C. B. Murray, R. G. Griffin, M. G. Bawendi, *J. Chem. Phys.* **100**, 3297 (1994).
11. V. Colvin *et al.*, *Nature* **370**, 354 (1994); B. O. Dabbousi *et al.*, *Appl. Phys. Lett.* **66**, 1316 (1995).
12. See, for example, D. J. Norris, A. Sacra, C. B. Murray, M. G. Bawendi, *Phys. Rev. Lett.* **72**, 216 (1994), and references therein.
13. B. O. Dabbousi, C. B. Murray, M. F. Rubner, M. G. Bawendi, *Chem. Mater.* **6**, 216 (1994).
14. G. S. H. Lee *et al.*, *J. Am. Chem. Soc.* **110**, 4863 (1988); N. Herron, J. C. Calabrese, W. E. Farneth, Y. Wang, *Science* **259**, 1426 (1993); T. Vossmeyer *et al.*, *ibid.* **267**, 1476 (1995).
15. We measured this by focusing on the carbon substrate at the edge of the domain and moving radially inward, counting discrete jumps in focal length.
16. J. V. Sanders, *Philos. Mag. A* **42**, 705 (1980); P. Bartlet, R. H. Ottwill, P. N. Pusey, *Phys. Rev. Lett.* **68**, 3801 (1992); M. D. Eldridge, P. A. Madden, D. Frenkel, *Nature* **356**, 35 (1993).
17. J. Th. G. Overbeek, *Adv. Colloid Interface Sci.* **15**, 251 (1982), and references therein.

18. M.G.B. thanks the David and Lucille Packard Foundation and the Sloan Foundation for fellowships. This research was funded in part by NSF grants DMR-91-57491 and ECS-91-18907 and by the NSF-MRSEC program (DMR-94-00034).

26 June 1995; accepted 29 September 1995

Creation of Theta-Auroras: The Isolation of Plasma Sheet Fragments in the Polar Cap

Patrick T. Newell* and Ching-I. Meng

The auroral oval is a ring of luminosity enclosing geomagnetic field lines connected to the solar wind. Occasionally the ring has a bar across it, which seems to imply a bifurcation of the open region. Here results confirm that this "θ-aurora" actually does represent this odd bifurcated configuration, and they demonstrate how it happens. It has hitherto been assumed that θ-auroras occur when the interplanetary magnetic field is directed northward, because that is true of most very-high-latitude arcs. In fact, θ-auroras occur exclusively during the dynamic reconfiguration that follows when the interplanetary magnetic field turns southward after a prolonged northward interval.

When imaged from space in ultraviolet (UV), the Earth wears a halo: A ring of luminosity termed the auroral oval encircles the magnetic poles and has a typical diameter of 36°. Frank, Craven, and co-workers (*1, 2*) have discovered a spectacular effect, namely that the UV image of the polar cap sometimes instead is that of a circle with a bar across it, a phenomenon termed the θ-aurora. The bar (a transpolar arc) runs in the noon-to-midnight direction. It has been suggested that the θ-aurora represents a bifurcation of the Earth's magnetotail plasma sheet, with an isolated splinter of tail plasma being surrounded by geomagnetic field lines that are open to the interplanetary magnetic field (IMF). Aside from the geometry of the images, this suggestion was motivated by ionospheric plasma flow observations indicating antisunward flow surrounding the transpolar arc but sunward flow within it. (Once a magnetic field line becomes connected to the IMF, the general motion of flow must be that of the solar wind, which is antisunward, but field lines in the plasma sheet flow toward the sun.)

However, the same imaging team has cautioned that the isolation of the central arc is not well established (*2*), and doubts about the uniqueness and character of the θ-aurora configuration abound. It is well established that most polar cap arcs occur under IMF $B_z > 0$ conditions (*3, 4*). Theoretically this is because if $B_z > 0$, the

Table 1. The IMF conditions when θ-auroras are first observed.

Date and time (UT)	IMP-8 observations of IMF
	Polar BEAR images
12/16/86 07:17	$B_z < 0$ in sheath after data gap
12/22/86 08:33	$B_z < 0$ after data gap
1/3/87 03:53	No IMF data. Polar cap empty by 04:30 and substorm before 05:40 UT
1/11/87 02:43	$B_z < 0$ after sustained interval > 0
1/15/87 02:57	Data gap, but about 10 min earlier $B_z < 0$ after $B_z > 0$
1/17/87 00:29	$B_z < 0$ after fluctuating about 0
1/27/87 01:58	$B_z > 0$ weakly after variable IMF
2/26/87 01:06	Variable B_z in sheath after $B_z > 0$
3/2/87 03:07	IMP-8 and DMSP F7 data gap
	DE-1 cases reported in literature
10/17/81 17:00	No IMF
10/31/81 22:45	$B_z < 0$ after interval of $B_z > 0$
11/8/81 15:45	No IMF
11/25/81 11:30	No IMF
8/3/86 17:45	$B_z < 0$ after interval of $B_z > 0$

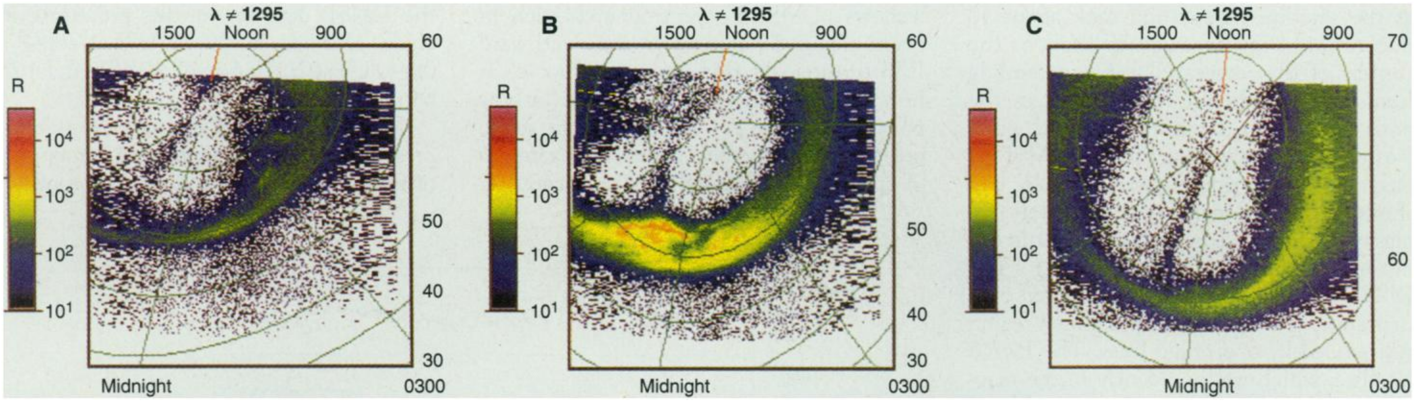

Fig. 1. UV images of the northern polar regions from space at 1295 ± 15 Å made with the Polar BEAR satellite imager (the latitude–local time grid is based on the magnetic rather than geographic pole). Times given refer to magnetic local time. Numbers at right of each panel label the lines of magnetic latitude. The images are from three consecutive passes on 11 January 1987 over the northern polar regions: (**A**) 02:43 UT, (**B**) 04:29 UT, and (**C**) 06:14 UT. R, rayleighs. Most of the auroral oval is visible, as well as a transpolar arc (the θ-aurora). In (C), the DMSP F7 satellite trajectory is shown as a black line, with bars showing the location of plasma sheet precipitation.

amount of open geomagnetic flux in the polar cap should be reduced. It has been observationally established that the plasma sheet expands into the polar cap along the dawn and dusk flanks when $B_z > 0$ (*3*). As a result, configurations that somewhat resemble the θ-aurora can exist, but they do not imply any bifurcation of the region of field lines that are open to the IMF (*5*).

It is widely assumed that θ-auroras are also a phenomenon produced by northward IMF conditions. This assumption, which has even reached introductory textbooks (*6*), apparently stems from the belief that the θ-aurora must represent some variant of better-established polar cap arc phenomena. Interestingly, the one θ-aurora discussed in the literature for which IMF data have been reported occurred during southward IMF ($B_z < 0$) conditions after an extended interval of northward IMF (*2*), a fact that has not altered in the slightest the prevalent association of θ-auroras with northward IMF. It has been difficult to further investigate the phenomenology of θ-auroras, primarily because of the paucity of UV images of the Earth from space (and secondarily because of the spottiness of IMF coverage).

We use data from unpublished UV images to demonstrate that the above assumptions about θ-auroras are unwarranted. θ-auroras prove to occur, apparently exclusively, under southward IMF conditions after a period of northward IMF causes a traditional expansion of the plasma sheet into the polar cap. Moreover, a unique mechanism exists that produces highly isolated strips of plasma sheet in the polar cap (the configuration originally hypothesized by Frank). A simple model is presented here that explains the observed motion of the transpolar arc across the polar cap and its dependence on IMF sector structure.

We analyzed UV images of high-latitude regions taken by the Polar BEAR satellite (*7*), as well as charged particle precipitation observations from the Defense Meteorological Satellite Program (DMSP) satellites F6 and F7. Instruments on these flights included curved-plate electrostatic analyzers that measured electrons and ions from 32 eV to 30 keV (*8*). The DMSP satellites are three-axis stabilized, with the detector apertures pointed always toward the zenith, so that at polar latitudes only particles that are well within the atmospheric loss cone are observed.

We examined each image in the Polar BEAR collection and found nine cases of apparent θ-auroras. Figure 1 shows images from three consecutive orbits (counted as one event) taken on 11 January 1987. Images were formed by a sweeping line scanner

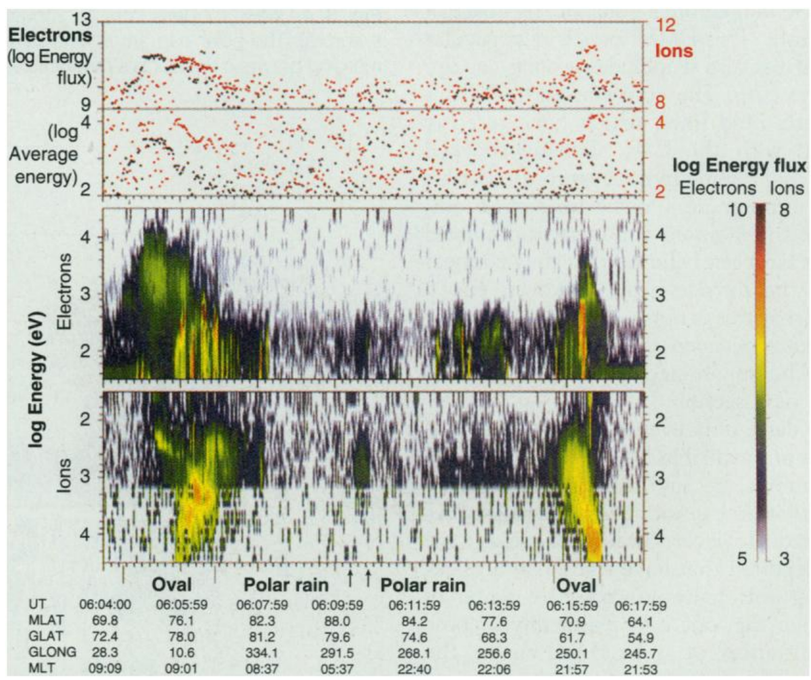

Fig. 2. A spectrogram showing precipitating electrons and ions from a DMSP F7 satellite pass through the polar regions at the time shown in Fig. 1C. In the top portion of the figure, the upper line plot shows log total energy flux in electron volts per square centimeter per second per steradian, and the lower line plot shows log average energy in electron volts. The color scale is calibrated in differential energy flux (electron volts per square centimeter per second per steradian per electron volt). Arrows at bottom denote the magnetotail-type plasma that was found isolated by apparently open field lines (those containing only polar rain precipitation). MLAT, magnetic latitude; GLAT, geographic latitude; GLONG, geographic longitude; MLT, magnetic local time. The image was formed with a filter centered at λ = 1295 Å, but the auroral emission measured is the oxygen λ 1304 Å line.

Johns Hopkins University Applied Physics Laboratory, Laurel, MD 20723, USA.

*To whom correspondence should be addressed.

as the satellite moved and took about 10 min to form; the times given apply to the centers of the images. The bar extending from before midnight to noon across the polar cap is the θ-aurora. Figure 2 gives particle precipitation data from a DMSP F7 pass made at the time shown in Fig. 1C and shows an isolated region of magnetotail-like plasma surrounded by polar rain (soft homogeneous electron precipitation). The DMSP data thus support the proposed configuration of the θ-aurora as a closed region surrounded by open field lines. The IMP-8 satellite, which was apparently in the magnetosheath, indicated that the IMF had turned southward from a northward direction before the first appearance of a θ-aurora. The combined Polar BEAR, DMSP, and IMP-8 data for this event show a scenario typical for θ-aurora events as a whole in our investigation: The θ-aurora occurs after the IMF turns southward, and the DMSP data indicate that the θ-aurora represents magnetotail plasma surrounded by open field lines (polar rain or no precipitation). Table 1 summarizes these observations, as well as listing IMF data for the events reported by the DE-1 satellite imaging team for reference.

One more observational result is key to understanding the θ-aurora phenomenon. Figure 3 shows a DMSP F7 spectrogram from 15 January 1987, taken at 02:18 UT, about 30 min before a Polar BEAR image of a θ-aurora. This DMSP pass is of particular interest because it includes a polar cap arc and the cusp. The cusp consists of Earth's magnetic field lines, which have recently merged with the IMF, allowing shocked solar wind plasma free access to the Earth's upper atmosphere. On the basis of DE images of the θ-aurora and other sun-aligned arcs, it has been believed that they connect up to the dayside oval. However, Fig. 3 shows that this is not quite correct: A clear gap exists between the polar arc and the cusp. The importance of this becomes clear in the next section.

To date, only events whose global UV images are available have been considered as θ-auroras, because otherwise the global configuration cannot be unambiguously determined. However, because no events have been reported that have transpolar arcs extending only halfway across the center of the polar cap, one may reasonably suppose that instances of isolated plasma in the polar cap are θ-auroras. To further test our model, we examined a few cases for which continuous IMF and DMSP F6 and F7 precipitation coverage was available and for which the IMF changed to a southward direction after being at least several nT positive for several hours. Several of the examples we investigated showed isolated plasma in the center of the polar cap. Figure 4 shows a DMSP F7 spectrogram of such an event about 20 min after the southward IMF turning. At this stage, it is not clear how long the IMF must be positive (or how positive it must be) for a θ-aurora to be created. (For reference, additional examples of apparent θ-auroras that were located in the DMSP data set by this procedure include 12/24/83 at 09:30 UT; 1/28/84 at 09:40 UT; 02/24/84 at 10:10 UT; and 4/25/84 at 14:00 UT.)

Figure 5 illustrates the scenario that the present observations support. After a period of northward IMF, the polar cap contracts

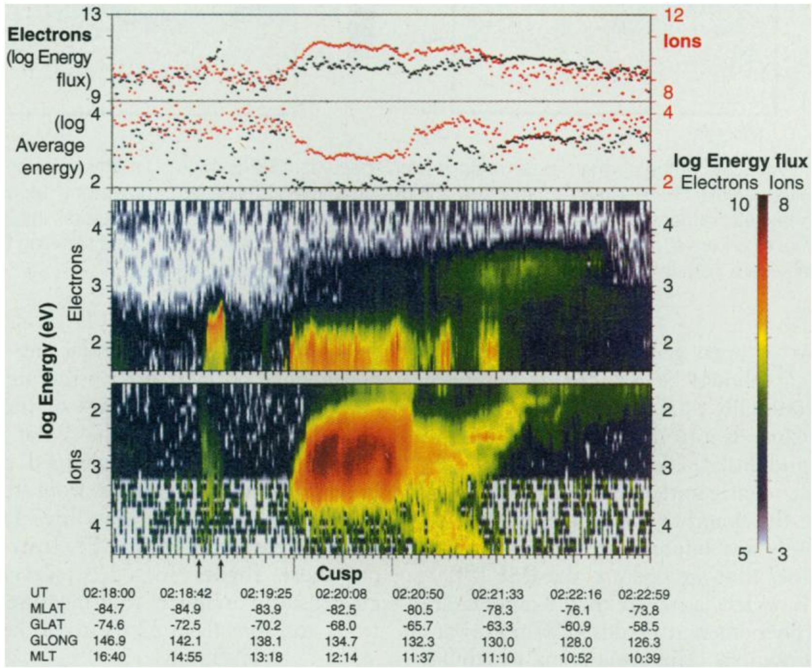

Fig. 3. A DMSP F7 pass from 15 January 1987 at 02:20 UT (about 35 min before the formation of a θ-aurora). The polar cap arc shown by arrows does not connect up to the cusp, which is the site of merging between the Earth's magnetic field and the IMF. Terminology is defined as in Fig. 2.

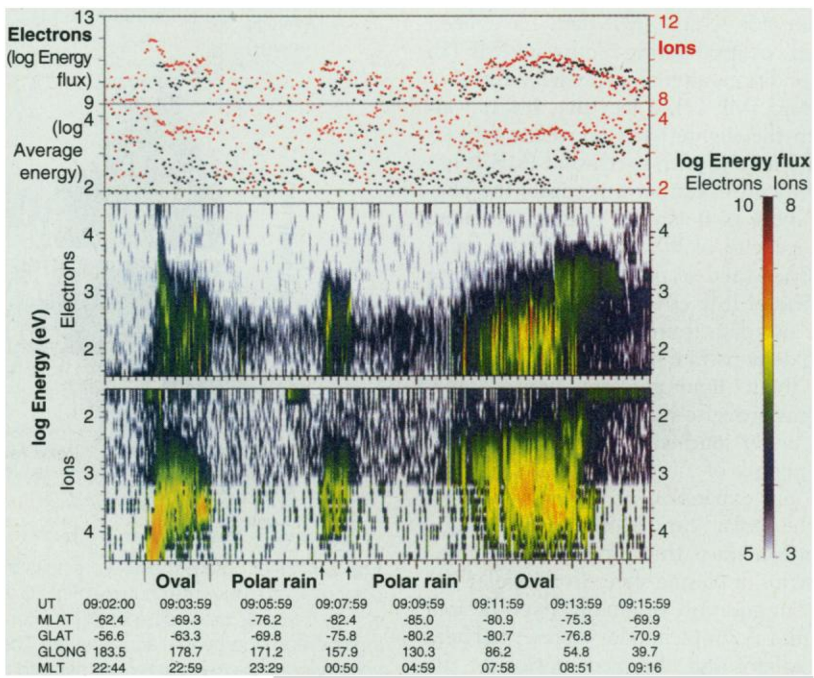

Fig. 4. A sample DMSP F7 pass we selected by looking for intervals of southward IMF after prolonged intervals of northward IMF is shown. An isolated arc in the middle of the polar cap is presumably a θ-aurora; on both sides of the arc polar rain exists, indicating open field lines. Terminology is defined as in Fig. 2.

as magnetospheric field lines disconnect from the IMF; or equivalently, the plasma sheet along the dawn and dusk flanks of the oval expands into the polar cap (*3*). Along the boundary between open and closed field lines a velocity shear exists (say between sunward convection within the oval and antisunward convection further poleward) so that a sun-aligned arc often forms at the interface. However, the arc does not quite extend to the cusp. When the IMF turns southward, rapid merging and convection tailward of magnetic flux resume at the cusp location.

There is ample theoretical (*9*) and observational evidence (*10, 11*) to support the conclusion that as flux becomes connected to the IMF, it usually convects around the polar cap circumference at the boundary between open and closed field lines, with the direction of preferred convection being determined by the IMF B_y. The overall motion is antisunward, but the predominant motion is azimuthal. For $B_y > 0$ in the Northern Hemisphere, the direction of convection is toward dawn. Hence the newly opened flux is added to the flanks of the oval inside the existing sun-aligned arc. This gradually leads to the arc becoming separated from the oval and convecting toward higher latitudes. Only after >10 min of southward IMF conditions does the arc become a true θ-aurora: a bifurcation of the polar cap.

This simple model predicts that θ-auroras should appear to move from the dawn side toward the dusk side for $B_y > 0$ in the Northern Hemisphere, and from the dusk side toward the dawn side in the Southern Hemisphere. The one instance in which θ-auroras were imaged in both hemispheres (*2*) showed precisely this effect. Our model further predicts that if the IMF turns northward again after a θ-aurora is formed, the motion should stop. No data are currently available for investigation of this prediction. The model also implies that long-duration θ-aurora events (several hours) should occur only when the IMF B_z component changes sign every hour or two, as was the case for the long-lived event shown in Fig. 1.

Because of the scheduled launch of the Polar satellite in December 1995, which will include suitable imagers, there soon should be ample opportunity to test our model in detail. The data presented here show that θ-auroras do represent a true isolation of magnetotail plasma in the polar cap (*12*) and that they are formed only when the IMF turns southward after an extended period of northward conditions.

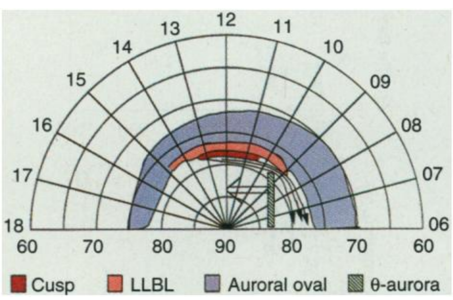

Fig. 5. A simple model illustrating the formation of a θ-aurora. Under northward IMF conditions, polar cap arcs form at the interface between open and closed field lines, but these arcs do not connect up to the polar cusp. When the IMF turns southward and flux is transferred from the dayside to the nightside, the flux is convected along the polar cap boundary and is added to the flanks of the oval inside the arc, pushing the latter to higher latitudes. LLBL, low-latitude boundary layer.

REFERENCES AND NOTES

1. L. A. Frank *et al.*, *J. Geophys. Res.* **91**, 3177 (1986).
2. J. D. Craven *et al.*, *Geophys. Res. Lett.* **18**, 2297 (1991).
3. C.-I. Meng, *ibid.* **8**, 273 (1981).
4. S. Ismail and C.-I. Meng, *Planet. Space Sci.* **30**, 319 (1982).
5. E. W. Hones *et al.*, *Geophys. Res. Lett.* **16**, 37 (1989).
6. J. K. Hargreaves, *The Solar-Terrestrial Environment*, (Cambridge Univ. Press, Cambridge, 1992).
7. The history of the Polar BEAR satellite includes 25 years spent hanging from the ceiling of the Smithsonian Air and Space Museum before being reclaimed and refurbished for launch. More detail can be found in the special issue of the *Johns Hopkins APL Technical Digest* devoted to Polar BEAR (**8**, issue 3, 1987).
8. D. A. Hardy, *Rep. AFGL-TR-84-0317* (Air Force Geophysics Laboratory, Hanscom Air Force Base, Boston, MA, 1984).
9. D. J. Southwood, *J. Geophys. Res.* **92**, 3207 (1987).
10. R. A. Heelis, *ibid.* **89**, 2873 (1984).
11. J. P. Heppner and N. C. Maynard, *ibid.* **92**, 4467 (1987).
12. J. M. Weygand *et al.* (unpublished manuscript) have used the Viking UV imager and automated identifications from the DMSP database to conclude that some polar cap arcs are surrounded by open field lines (polar rain).

13. Supported by NSF grant ATM-9322435 to the Johns Hopkins University Applied Physics Laboratory. D. Hardy and colleagues designed and built the DMSP particle detectors and were generous in sharing data. R. E. Huffman was principal investigator on the Polar BEAR UV imager.

4 May 1995; accepted 6 September 1995

Fission Track Evidence on the Initial Rifting of the Red Sea: Two Pulses, No Propagation

Gomaa I. Omar and Michael S. Steckler

Fission track analyses indicate that the Red Sea initially opened simultaneously along its entire length. Two distinct pulses of uplift and erosion characterized the early stages of rifting in the Red Sea throughout Egypt and in southwestern Saudi Arabia. The first pulse began at ~34 million years ago (Ma). The second pulse began in the early Miocene (21 to 25 Ma) and marked the start of the main phase of extension. These data support a rigid plate model for continental extension. These results also indicate that the initiation of rift flank uplift, and therefore rifting, and volcanism occurred nearly simultaneously. This conflicts with classical models of active and passive extension that predict sequential development of these features.

The Red Sea, with the Gulf of Aden, is the only young example of the splitting of a continent to create a new ocean basin. At present the mode of extension in the Red Sea varies from well-established oceanic accretion in the south to late stage continental rifting in the north (*1, 2*) (Fig. 1). The along-strike contrasts in the Red Sea provide evidence for south to north propagation for the initiation of sea floor spreading (*3, 4*).

It is not known, however, whether the initiation of rifting underwent a similar south to north progression. Rigid plate kinematics requires that motion begins simultaneously over the entire length of the Red Sea (Fig. 2). The resulting initiation of a rift valley, and later changes in the opening rate, would occur virtually simultaneously along the length of the Red Sea. In contrast, if the opening of the Red Sea initialized as an unzipping from south to north (Fig. 2), then internal deformation of the plate is required. How well continental breakup is approximated by rigid plate tectonics can be evaluated by examining whether the initiation of continental rifting was synchronous or propagated.

Apatite fission track (FT) analysis has proved to be a powerful tool in studying the timing, magnitude, and geometry of uplift and erosion events of the Red Sea rift flanks (*5–8*). In the Gulf of Suez, FT analyses of apatites from Precambrian crystalline rocks along its western margin have established that large-scale erosion of the uplifted rift flank began at 21 ± 2 Ma, coeval with the

G. I. Omar, Geology Department, University of Pennsylvania, 240 South 33rd Street, Philadelphia, PA 19104, USA.
M. S. Steckler, Lamont-Doherty Earth Observatory, Palisades, NY 10964, USA.